Theoretical Investigation on Stability and Isomerizations of CH_3SO Isomers

Xiaoyan Li,[†,§] Hongmin Fan,[†,‡] Lingpeng Meng,[†] Yanli Zeng,[†] and Shijun Zheng*[,†]

Institute of Quantum Chemistry at College of Chemistry, Hebei Normal University, Shijiazhuang, 050016, P. R. China, Tianjin Institute of Power Sources, Tianjin, 300381, P. R. China, and Department of Chemistry, Graduate School, Chinese Academy of Sciences, Beijing, 100049, P. R. China

Received: November 10, 2006; In Final Form: December 29, 2006

The stability and isomerizations of CH_3SO isomers have been investigated at B3LYP/6-311G(d,p), MP2/6-311G(d,p), QCISD/6-311G(d,p), and CCSD(T)/6-311G(d,p) levels. Geometries of isomers and transition states (TS) have been optimized at the B3LYP/6-311G(d, p) level. Vibration analysis and the intrinsic reaction coordinate (IRC) calculated at the same level have been applied to validate the connection of the stationary points. The four different methods give similar results: 11 isomers and 9 isomerization channels were found. CH_3SO and $CH_2(S)OH$ are the most stable species among the 11 isomers. Furthermore, the breakage and formation of the chemical bonds in isomerization reactions have been discussed by the topological analysis method of electronic density. The "energy transition state (ETS)" and the "structure transition state (STS)" of all the isomerizations have been found. The topological analysis shows that the relative positions of ETS and STS are determined by reaction energy. The nonplanar four-member ring structure transition state (STS), which was first found in this paper, extended the concept of ring STS.

1. Introduction

With the rapid rise of economic development, acid rain has become one of the ten most serious problems which threaten the world environment. CH_3SO has been postulated as one of the key intermediates in the DMS oxidation mechanism.[1−3] It may play an important role in the formation of acid rain because the bond length of the C−S bond is longer than that in CH_3S.[4] The principal mechanism of SO_2 formation has been suggested to include a sequence of reactions of the CH_3SO radical with O_2, NO_2, and O_3 as well as the thermal decomposition of CH_3-SO_2.[2,3] The properties and the reaction of the CH_3SO radical with NO_2 and O_3 have been studied by several groups.[5−10] Until now, however, there has been no theoretical or experimental study on the stability and isomerizations of CH_3SO isomers. Thus, a detailed knowledge about structure, stability, bonding, and isomerization properties of various CH_3SO isomers is very desirable and helpful for controlling the formation of acid rain. In order to gain some insight into the character of CH_3SO isomers, in this paper, the stability and isomerization reaction are investigated theoretically. The breakage and formation of the bonds in the isomerization reaction paths have been discussed. The structure transition state and the structure transition region of the isomerization reaction have been found. The relationship between the topological characteristic of density distribution and the energy variation along the reaction path has also been discussed. We hope that our computations may provide useful information for understanding the properties of the CH_3SO radical and stimulate further studies on it.

* Author to whom correspondence should be addressed at Institute of Computational Quantum Chemistry, College of Chemistry, Hebei Normal University, Yuhua Road, Shijiazhuang, 050016, P. R. China. Tel/Fax: +86 311 86269217. E-mail: sjzheng@mail.hebtu.edu.cn .

† Hebei Normal University.

‡ Tianjin Institute of Power Sources.

§ Chinese Academy of Sciences.

2. Computational Methods

The geometries of CH_3SO isomers and transition states and some points on the potential energy surface were located by B3LYP/6-311G(d,p) calculations with second-order MP2/6-311G(d,p), QCISD/6-311G(d,p), and CCSD(T)/6-311G(d,p) energy corrections. Harmonic frequencies were calculated to characterize the stationary points. Starting from the transition state, the reaction paths have been followed using Fukui's theory of intrinsic reaction coordinate (IRC) method[11] in mass-weighted internal coordinates going in forward and reverse directions from the transition state with the step size equal to 0.01 $(amu)^{1/2}$ bohr. In this work, the reaction paths were traced out by the mass-weighted internal coordinate (*S*), which is more precise than a single distance or an angle.[12,13] Computations were performed using the GAUSSIAN 98 program.[14] Molecular graph and gradient path of electronic density of some points in the reaction are plotted by program AIM 2000.[15]

3. Results and Discussion

3.1. Isomers. We did a lot of work to search for possible isomers on a potential energy surface considering diversified structural and conformational isomeric forms. Eleven isomers are found to be energy minima with all real vibrational frequencies. They are CH_3SO, $CH_2(S)OH$, CH(OH)SH(1), CH-(OH)SH(2), CH_3OS, $CH_2(O)SH(1)$, $CH_2(O)SH(2)$, $CH_2(O)SH(3)$, $CH_2S(O)H$, and CH_2OSH. In these 11 isomers, CH(OH)SH(1), CH(OH)SH(2) are two different structures of CH(OH)SH, and $CH_2(O)SH(1)$, $CH_2(O)SH(2)$, $CH_2(O)SH(3)$ are three different structures of $CH_2(O)SH$. In order to discuss the isomerization of the 11 isomers, 9 interconversion transition states are found to have and only have one image vibrational frequency. The geometry parameters of isomers and transition states (TS) on the reaction potential energy surface are optimized and shown in Figure 1. The corresponding energies are listed in Table 1. The reaction potential energy surfaces are shown in Figure 2.

10.1021/jp067435e CCC: $37.00
Published on Web 03/03/2007

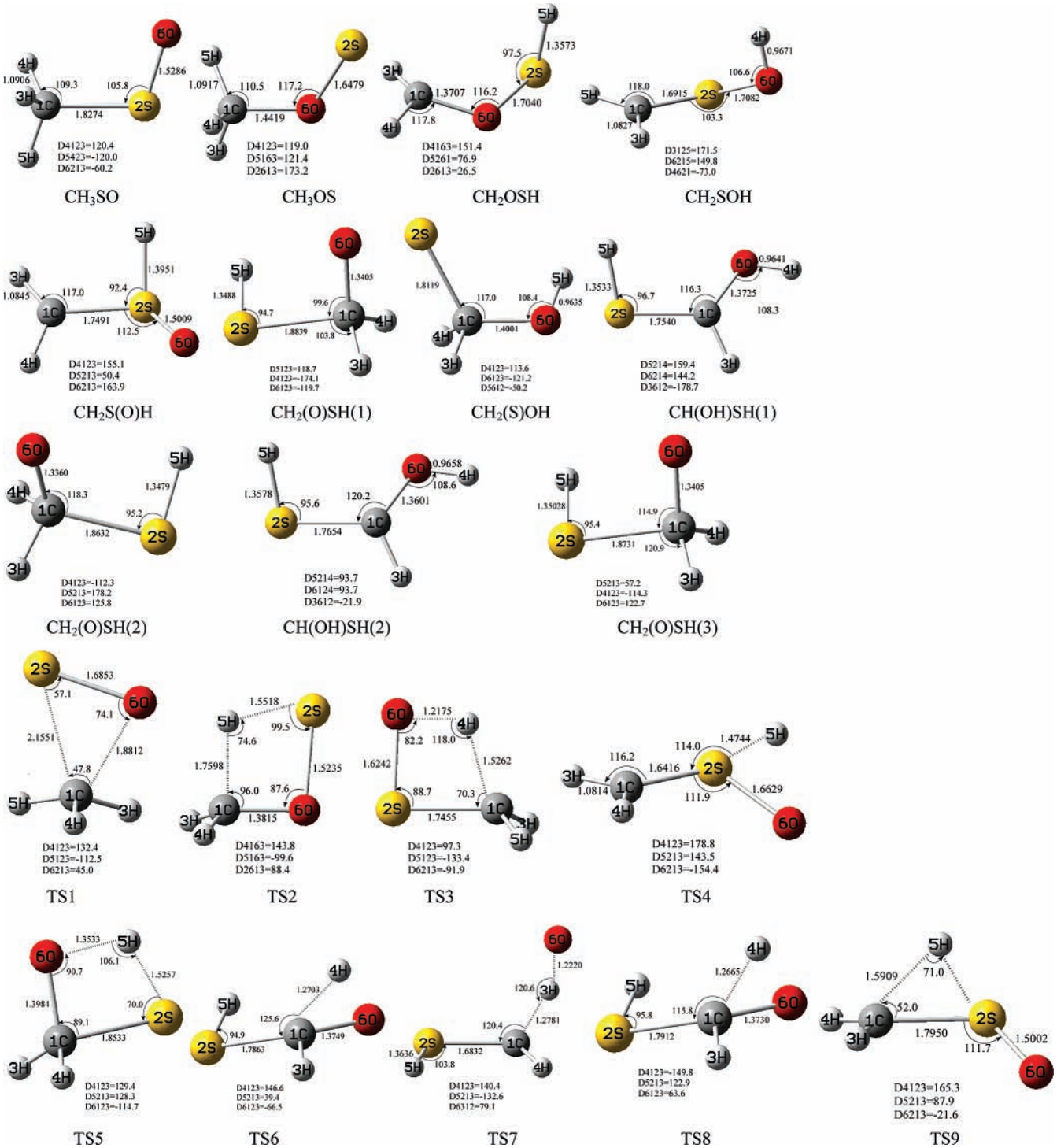

Figure 1. Geometries of the isomers and transition states (bond length: Å; bond angle and dihedral angle: degree(°)).

From Table 1, it appears that some disagreements between the order of energies of the obtained 11 isomers do exist for the B3LYP/6-311G(d,p), QCISD/6-311G(d,p) and CCSD(T)/6-311G(d,p) and MP2/6-311G(d,p) methods. However, it is evident that the QCISD/6-311G(d,p) and CCSD(T)/6-311G(d,p) energies orderings of the obtained 11 isomers are in general agreement with that of MP2/6-311G(d,p). CCSD(T)/6-311G(d,p) energies are to be used in the following discussion.

Generally, the species with lower total energy has higher thermodynamical stability. Thus, the theromodynamical stability order for these isomers is $CH_2(S)OH$ (−18.9) > CH_3SO (0.0) > CH(OH)SH(2) (22.0) > CH(OH)SH(1) (27.5) > CH_3OS (43.0) > $CH_2(O)SH(1)$ (65.8) > $CH_2(O)SH(2)$ (69.2) > $CH_2(O)SH(3)$ (76.3) > CH_2SOH (86.6) > CH_2OSH (146.6) > $CH_2S(O)H$ (218.5). The values in parentheses are relative energies in kJ/mol with reference to CH_3SO. It is very clear that $CH_2(S)OH$ and CH_3SO are the most stable geometries; CH_2OSH and $CH_2S(O)H$ are unstable compared to other isomers because of their high relative energy.

Nine interconversion transition states are obtained, and their structures are shown in Figure 1. By means of isomers and transition states, a schematic PES is plotted in Figure 2.

As shown in Figures 1 and 2, the lowest-lying $CH_2(S)OH$ and $CH_2(O)SH(1)$ can convert easily to each other via TS5 for which the energy is 143.7 kJ/mol, but notice that the energy of $CH_2(O)SH(1)$ is 84.7 kJ/mol higher than that of $CH_2(S)OH$, It

TABLE 1: Energies (E_{ele}), Zero-Point Energy Correction (ZPE), and Relative Energy (E_{rel}) for the Various Compounds

	total energy (E_{ele}) (a.u.)						relati ve energ y (E_{rel}) (kJ/mol)			
species	B3LYP	ZPE (a.u.)	B3LYP(co rr)	MP2	QCISD	CCSD(t)	B3LYP	MP2	QCIS D	CCSD(t)
CH_3SO	−513.3 332	0.0399	−513.2933	−512.4 497	−512.4 888	−512.5 041	0.0	0.0	0.0	0.0
CH_3OS	−513.3 163	0.0416	−513.2747	−512.4 391	−512.4 734	−512.4 877	48.8	27.8	40.4	43.0
CH_2OSH	−513.2 750	0.0361	−513.2389	−512.3 983	−512.4 338	−512.4 482	142.7	134. 8	144.3	146.6
CH_2SOH	−513.2 984	0.0379	−513.2605	−512.4 215	−512.4 560	−512.4 711	86.0	74.0	86.0	86.6
$CH_2S(O)H$	−513.2 490	0.0356	−513.2134	−512.3 729	−512.4 056	−512.4 208	209.6	201. 4	218.2	218.5
$CH_2(O)SH$(1)	−513.3 053	0.0380	−513.2672	−512.4 217	−512.4 649	−512.4 790	68.4	73.4	62.7	65.8
$CH_2(S)OH$	−513.3 338	0.0416	−513.2923	−512.4 649	−512.4 972	−512.5 113	2.6	−39. 9	−22.0	−18.9
CH(OH)SH (1)	−513.3 168	0.0376	−513.2792	−512.4 458	−512.4 792	−512.4 936	37.0	10.2	25.2	27.5
$CH_2(O)SH$(2)	−513.3 038	0.0361	−513.2677	−512.4 226	−512.4 642	−512.4 777	67.1	71.0	64.5	69.2
CH(OH)SH (2)	−513.3 197	0.0374	−513.2823	−512.4 479	−512.4 812	−512.4 957	28.8	4.7	19.9	22.0
$CH_2(O)SH$(3)	−513.3 020	0.0356	−513.2664	−512.4 193	−512.4 616	−512.4 750	70.6	79.7	71.3	76.3
TS1	−513.2 151	0.0382	−513.1769	−512.3 166	−512.3 656	−512.3 822	305.3	349. 1	323.1	319.7
TS2	−513.2 361	0.0342	−513.2019	−512.3 542	−512.3 895	−512.4 066	239.7	250. 5	260.4	255.7
TS3	−513.2 463	0.03447	−513.2119	−512.3 476	−512.4 002	−512.4 165	213.5	267. 8	232.4	229.8
TS4	−513.2 047	0.0325	−513.1722	−512.3 111	−512.3 522	−512.3 714	317.6	363. 5	358.3	348.1
TS5	−513.2 761	0.0355	−513.2406	−512.3 934	−512.4 322	−512.4 493	138.2	147. 7	148.4	143.7
TS6	−513.2 553	0.0328	−513.2226	−512.3 773	−512.4 124	−512.4 290	185.4	189. 9	200.4	197.0
TS7	−513.1 765	0.0300	−513.1465	−512.2 748	−512.3 075	−512.3 468	385.5	458. 8	475.5	412.6
TS8	−513.2 536	0.0327	−513.2209	−512.3 753	−512.4 108	−512.4 273	189.9	195. 1	204.6	201.4
TS9	−513.2 231	0.0331	−513.1900	−512.3 433	−512.3 749	−512.3 927	271.0	279. 1	298.7	292.2

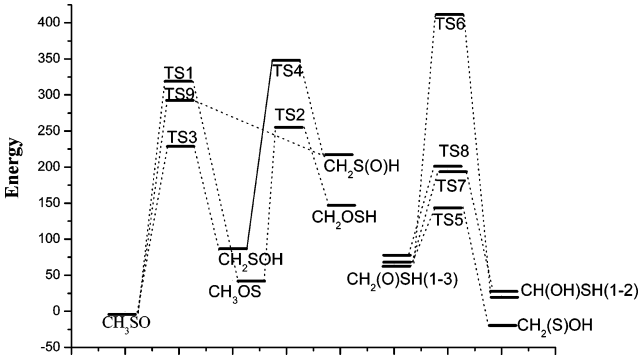

Figure 2. Schematic potential energy surface of CH_3SO system at CCSD(T)/6-311G(d,p) level.

is easier for $CH_2(O)SH(1)$ to convert to $CH_2(S)OH$, so $CH_2(S)OH$ is the most stable. CH_3SO could convert to CH_3OS, CH_2SOH, and $CH_2S(O)H$ via the energy barrier of 319.7, 229.8, and 292.2 kJ/mol, respectively. Because of the high energy barrier and because the energies of CH_3OS, CH_2SOH, and $CH_2S(O)H$ are all higher than that of CH_3SO, CH_3SO should exist stably and may be experimentally observed. The third stable isomers are CH(OH)SH(1) and CH(OH)SH(2); CH(OH)SH(1) can convert to $CH_2(O)SH$ (2) via TS6 and TS7 and CH(OH)SH(2) can convert to $CH_2(O)SH$ (3) via TS8, because of the high isomerization barriers of TS6−8 and because the energy of $CH_2(O)SH$ (2) and $CH_2(O)SH$ (3) are 41.7 and 54.3 kJ/mol higher than those of CH(OH)SH(1) and CH(OH)SH(2), respectively. CH(OH)SH(1) and CH(OH)SH(2) should be stable too.

As discussed above, $CH_2(S)OH$, CH_3SO, CH(OH)SH(1), and CH(OH)SH(2) are more stable than other isomers. The energies of other isomers are higher than those of these four isomers, especially the energies of CH_2OSH and $CH_2S(O)H$ are 146.6 and 218.5kJ/mol higher than that of CH_3SO, respectively. Because of the higher energies of the two isomers, CH_2OSH and $CH_2S(O)H$ are unstable.

3.2. Topological Analyses of Electronic Density on IRC Paths. Topological studies on reaction paths can provide very useful information about the reaction. And topological studies on some typical reactions have been carried out by some authors in recent years.[16−17] For each isomerization reaction, the topological analysis was carried out on the electronic density of some points along the reaction path. The potential energy curves of all reactions are listed in Figure 3. The ETS, STS, and transition state region are also found and listed in Figure 3.

3.2.1. Changes in Structure Determined by the Topology of the Electron Density. According to the topological analysis of electronic density in the theory of AIM,[18,19] electron density $\rho(r_c)$ is used to describe the strength of a bond and Laplacian of the electron density ($\nabla^2\rho(r_c)$) describes the characteristic of the bond. In general, the larger the value of $\rho(r_c)$, the stronger the bond. The field of $\nabla^2\rho(r_c) < 0$ is a charge-accumulated area, and $\nabla^2\rho(r_c) > 0$ is a charge-dispersed area. The Laplacian $\nabla^2\rho(r_c)$ is the sum of λ_1, λ_2, and λ_3, and λ_i is one of the eigenvalues of the Hessian matrix of electronic density. If a critical point has two negative and one positive eigenvalue, it is called (3, −1) or the bond critical point (BCP). If a critical point has two positive and one negative eigenvalue, it is called (3, +1) or the ring critical point (RCP), which indicates that a ring structure exists.

In the nine isomerization reaction, a three-membered ring transition structure, a four-membered ring transition structure, and a T-shape transition structure exist in $CH_3SO \xrightarrow{TS1} CH_3OS$, $CH_3OS \xrightarrow{TS2} CH_2OSH$, and $CH(OH)SH(1) \xrightarrow{TS7} CH_3(O)SH(2)$, respectively. The Topological properties are listed in Tables 2−4 for every reaction, respectively. Gradient paths of the electronic density or the molecular graph are plotted for some points along the reaction path and displayed in Figures 4−6, respectively.

In the $CH_3SO \rightarrow CH_3OS$ process, the electronic density $\rho(r_c)$ at the BCP of the C−S bond becomes smaller and smaller, which indicates that the C−S bond becomes weaker and weaker, and at last it is broken. The Laplacian $\nabla^2\rho(r_c)$ at the BCP of the C−S bond increased from −0.2829 to 0.1061, which shows that the character of the C−S bond turns from covalent to ionic. As the reactions proceed, the $\rho(r_c)$ at the BCP of the C−O bond becomes larger and larger, which indicates that the C−O bond becomes stronger and stronger, and then CH_3OS comes into being. The change of Laplacian $\nabla^2\rho(r_c)$ at the BCP of the C−O bond shows that the ionic C−O bond turns to a covalent bond in CH_3OS.

For the $CH_3SO \rightarrow CH_3OS$ process, from CH_3SO to $S_a = -0.74$, the C−S bond path becomes more and more bent. In the region of $S_a = -0.73$ to $S_a = +0.34$, the RCP appears, and

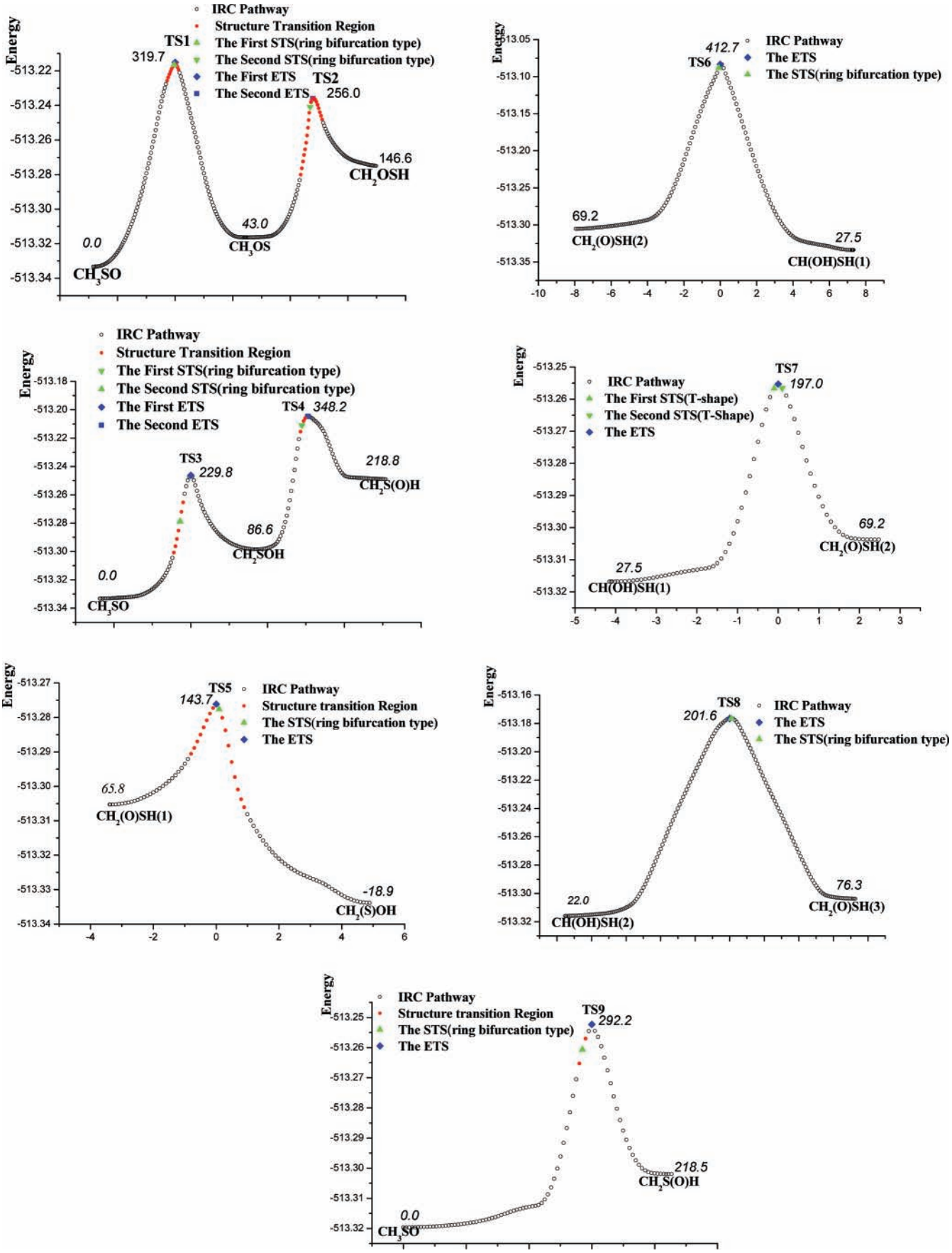

Figure 3. Potential energy curves of the isomerization reactions.

a C−O−S three-membered ring exists. As the reaction proceeds, the λ_2 eigenvalue of the RCP increases, and at the point of $S_a = -0.06$, it reaches a maximum. After the point of $S_a = -0.06$, the λ_2 eigenvalue of the RCP begins to decrease. From $S_a = +0.35$, the C−S bond disappears and then the C−O bond becomes stronger, and then CH_3OS forms.

TABLE 2: Topological Characters of BCP and RCP of the Ring Transition Region on the $CH_3SO \rightarrow CH_3OS$ Pathway

			eigenvalues of the Hessian Matrix			
bond	$S^{a,b}$	ρ	λ_1	λ_2	λ_3	$^2\rho^c$
RCP	−0.73	0.0688[d]	−0.0818	0.0079[d]	0.2886	0.2147
	−0.50	0.0698	−0.0836	0.0210	0.2697	0.2070
	−0.40	0.0710	−0.0857	0.0368	0.2467	0.1977
	−0.30	0.0720	−0.0873	0.0489	0.2273	0.1890
	−0.20	0.0728	−0.0886	0.0599	0.2093	0.1806
	−0.10	0.0735	−0.0894	0.0690	0.1927	0.1723
STS	−0.06	0.0742	−0.0898	0.0790	0.1662	0.1553
ETS	0.00	0.0744	−0.0896	0.0769	0.1614	0.1487
	+0.10	0.0741	−0.0885	0.0660	0.1610	0.1386
	+0.20	0.0737	−0.0870	0.0497	0.1665	0.1292
	+0.34	0.0209[e]	−0.0133	0.0012[e]	0.0913	0.0792
C−O	CH_3SO					
	−0.73	0.0689[d]	−0.0813	−0.0075[d]	0.3074	0.2185
	−0.30	0.0742	−0.0897	−0.0414	0.3377	0.2066
	−0.06	0.0852	−0.1098	−0.0771	0.3533	0.1664
	0.00	0.0878	−0.1147	−0.0841	0.3545	0.1557
	+0.10	0.0917	−0.1222	−0.0947	0.3564	0.1395
	+0.20	0.0951	−0.1290	−0.1040	0.3577	0.1246
	+0.34	0.1002[e]	−0.1392	−0.1173[e]	0.3596	0.1032
	CH_3OS	0.2385	−0.4081	−0.3999	0.4216	−0.3865
C−S	CH_3SO	0.1813	−0.2935	−0.2698	0.2804	−0.2829
	−0.73	0.0925[d]	−0.1093	−0.1023[d]	0.2031	−0.0085
	−0.30	0.0877	−0.1018	−0.0896	0.1985	0.0071
	−0.06	0.0801	−0.0909	−0.0647	0.1953	0.0397
	0.00	0.0786	−0.0890	−0.0586	0.1951	0.0475
	+0.10	0.0764	−0.0861	−0.0484	0.1945	0.0608
	+0.20	0.0747	−0.0840	−0.0377	0.1937	0.0721
	+0.34	0.0726[e]	−0.0831	0.0053[e]	0.1839	0.1061
	CH_3OS					
S−O	CH_3SO	0.2493	−0.3820	−0.3210	1.1841	0.4811
	−0.73	0.1881	−0.2508	−0.2165	0.2620	−0.2052
	−0.30	0.1875	−0.2497	−0.2157	0.2622	−0.2032
	−0.06	0.1868	−0.2480	−0.2134	0.2642	−0.1971
	0.00	0.1868	−0.2477	−0.2127	0.2655	−0.1949
	+0.34	0.1865	−0.2460	−0.2097	0.2715	−0.1841
	CH_3OS	0.1891	−0.2248	−0.1998	0.4873	0.0627

[a] S: reaction coordinate in unit of $(amu)^{1/2}$ bohr. [b] A minus sign denotes reverse direction of the reaction; a plus sign denotes forward direction of the reaction. [c] $\nabla^2\rho$: Laplacian of electron density. [d] The formation of the ring structure with a singularity in the density. [e] The formation or annihilation of the ring structure with a singularity in the density.

TABLE 3: Topological Characters of BCP and RCP of the Ring Transition Region on the $CH_3OS \rightarrow CH_2OSH$ Pathway

			eigenvalues of the Hessian Matrix			
bond	$S^{a,b}$	ρ	λ_1	λ_2	λ_3	$^2\rho^c$
RCP	−1.01	0.0523[d]	−0.0587	0.0105[d]	0.2302	0.1820
	−0.80	0.0570	−0.0657	0.0694	0.2200	0.2237
	−0.60	0.0599	−0.0708	0.1122	0.2063	0.2476
	−0.40	0.0616	−0.0742	0.1486	0.1889	0.2633
	−0.30	0.0620	−0.0754	0.1636	0.1800	0.2682
STS	−0.24	0.0622	−0.0758	0.1683	0.1777	0.2702
	−0.15	0.0621	−0.0762	0.1618	0.1860	0.2716
ETS	0.00	0.0614	−0.0757	0.1447	0.1803	0.2493
	+0.20	0.0592	−0.0729	0.1177	0.2114	0.2562
	+0.50	0.0532	−0.0639	0.0675	0.2124	0.2160
	+0.77	0.0456[e]	−0.0543	0.0063[e]	0.2021	0.1541
C−O	CH_3OS	0.2385	−0.4081	−0.3999	0.4216	−0.3865
	−1.01	0.2647	−0.4910	−0.4772	0.4993	−0.4688
	0.00	0.2813	−0.5516	−0.5237	0.5997	−0.4757
	+0.77	0.2781	−0.5295	−0.4860	0.7109	−0.3047
	CH_2OSH	0.2699	−0.5108	−0.4378	0.8308	−0.1178
C−H	CH_3OS	0.2819	−0.7692	−0.7393	0.5407	−0.9677
	−1.01	0.2576[d]	−0.6532	−0.6342[d]	0.4872	−0.8002
	−0.50	0.1742	−0.3668	−0.3653	0.3694	−0.3627
	−0.24	0.1340	−0.2556	−0.2493	0.3192	−0.1857
	0.00	0.1029	−0.1798	−0.1670	0.2918	−0.0550
	+0.50	0.0589	−0.0835	−0.0569	0.2415	0.1011
	+0.77	0.0456[e]	−0.0554	−0.0060[e]	0.2041	0.1427
	CH_2OSH					
S−H	CH_3OS					
	−1.01	0.0523[d]	−0.0597	−0.0098[d]	0.2361	0.1665
	−0.50	0.0831	−0.1192	−0.1081	0.2832	0.0559
	−0.24	0.1082	−0.1751	−0.1668	0.2938	−0.0481
	0.00	0.1367	−0.2486	−0.2320	0.3014	−0.1792
	+0.50	0.1948	−0.4064	−0.3642	0.2906	−0.4800
	+0.77	0.2108[e]	−0.4461	−0.3929[e]	0.2594	−0.5796
	CH_2OSH	0.2150	−0.4495	−0.3857	0.2103	−0.6249
S−O	CH_3OS	0.1891	−0.2248	−0.1998	0.4873	0.0627
	−1.01	0.1681	−0.2564	−0.2082	0.2983	−0.1662
	0.00	0.1623	−0.2418	−0.1950	0.2925	−0.1443
	+0.77	0.1646	−0.2509	−0.2021	0.2978	−0.1552
	CH_2OSH	0.1781	−0.2492	−0.2040	0.2683	−0.1849

[a] S: reaction coordinate in unit of $(amu)^{1/2}$ bohr. [b] A minus sign denotes reverse direction of the reaction; a plus sign denotes forward direction of the reaction. [c] $\nabla^2\rho$: Laplacian of electron density. [d] The formation of the ring structure with a singularity in the density. [e] The formation or annihilation of the ring structure with a singularity in the density.

The three-membered ring structure also exists in the process of $CH_2SOH \xrightarrow{TS4} CH_2S(O)H$, $CH(OH)SH(1) \xrightarrow{TS6} CH_2(O)SH(2)$, $CH(OH)SH(2) \xrightarrow{TS8} CH_2(O)SH(3)$, and $CH_3SO \xrightarrow{TS9} CH_2S(O)H$. The "energy transition states", "structure transition structure", and "structure transition region" are shown in Figure 3.

In the $CH3OS \xrightarrow{TS2} CH_2OSH$ process, the electronic density $\rho(r_c)$ at the BCP of the C−H bond becomes smaller and smaller, and the electronic density $\rho(r_c)$ at the BCP of the S−H bond becomes larger and larger, which indicates that the C−H bond becomes weaker and weaker, and at last it is broken. In the meantime, the S−H bond becomes stronger and stronger, and then CH_2OSH comes into being. The Laplacian $\nabla^2\rho(r_c)$ at the BCP of the C−H bond increased from −0.9677 to 0.1427, which shows that the character of the C−H bond turns from covalent to ionic. The Laplacian $\nabla^2\rho(r_c)$ at the BCP of the S−H bond decreased from 0.1665 to −0.6249, which shows that the character of the S−H bond turns from ionic to covalent.

In the $CH_3OS \rightarrow CH_2OSH$ process, a C−O−S−H four-membered ring structure exists in the region of $S_b = -1.01$ to $S_b = +0.77$. The formation of the C−O−S−H four-membered ring structure occurs with the formation of a singularity in the density. That is, the density at the newly appearing BCP of the S−H bond and the RCP of the C−O−S−H ring have the same value at $S_b = -1.01$. From Table 4, it can be seen that the λ_2 eigenvalue of the BCP of the S−H bond and the associated curvature of the RCP of the C−O−S−H are closed to zero, and they have equal magnitude and opposite signs. In the region of $S_b = -1.01$ to -0.24, the λ_2 eigenvalue of the S−H BCP and the RCP decrease and increase, respectively. After the point of $S_b = -0.24$, the λ_2 eigenvalue of RCP begins to decrease. As the reaction gets to the point where the BCP of the C−H bond and the RCP merge to form another singularity in the density at the point $S_b = +0.77$. (From Table 3, it can be seen that the two curvatures will have almost equal magnitude and opposite signs.) Then, the λ_2 eigenvalue of the BCP of the C−H bond and the associated curvature of the RCP of the C−O−S−H ring are close to zero. After the point $S_b = +0.77$, the C−H bond is broken.

It is worth pointing out that the C, O, S, and H atoms which form the four-membered ring structures are not in the same plane as in the former study.[20,21] The C atom is displaced from the H−O−S plane by about 17.4 degrees. A similar four-membered ring structure exists in $CH_3SO \xrightarrow{TS3} CH_2SOH$ and

TABLE 4: Topological Characters of BCP and RCP of the Ring Transition Region on the CH(OH)SH(1) → CH_2(O)SH(2) Pathway

			eigenvalues of the Hessian Matrix			
bond	$S^{a,b}$	ρ	λ_1	λ_2	λ_3	$^2\rho^c$
C-O	CH(OH)SH(1)	0.2766	−0.5664	−0.4582	0.7087	−0.3160
	−0.50	0.2045	−0.3814	−0.3573	0.4185	−0.3201
	−0.30	0.1362	−0.2266	−0.2166	0.4248	−0.0184
	−0.20	0.0600	−0.0698	−0.0663	0.2393	0.1032
	−0.15	0.0515	−0.0581	−0.0347	0.2189	0.1260
	−0.12	0.0528	−0.0679	−0.0314	0.2260	0.1268
C−BCP(H−O)	−0.11	0.0555	−0.0754	−0.0446	0.2372	0.1171
C-H	−0.10	0.0592	−0.0847	−0.0585	0.2505	0.1073
	−0.05	0.0941	−0.1727	−0.1548	0.3551	0.0276
	0.00	0.1645	−0.3698	−0.3475	0.4293	−0.2880
	+0.10	0.2778	−0.7784	−0.7611	0.5891	−0.9503
	+0.20	0.2895	−0.8077	−0.8038	0.5860	−1.0256
	+0.30	0.2888	−0.8024	−0.7904	0.5785	−1.0143
	+0.40	0.2830	−0.7776	−0.7603	0.5586	−0.9793
	+0.50	0.2755	−0.7469	−0.7267	0.5427	−0.9309
	+0.60	0.2695	−0.7238	−0.7020	0.5328	−0.8930
	CH_2(O)SH(2)	0.2663	-0.7105	−0.6899	0.5286	−0.8718
H−O	CH(OH)SH(1)	0.3656	−1.7795	−1.7416	1.0168	−2.5043
	−0.50	0.3629	−1.7506	−1.6995	1.0039	−2.4463
	−0.20	0.3620	−1.7095	−1.6596	0.9964	−2.3727
	−0.11	0.3452	−1.6329	−1.5932	0.9686	−2.2575
	0.00	0.1596	−0.4118	−0.3768	0.7754	−0.0133
	+0.05	0.0933	−−0.1748	−0.1390	0.5089	0.1950
	+0.09	0.0662	−0.0968	−0.0511	0.3639	0.2120
O−BCP(C−H)	+0.10	0.0630	−0.0868	−0.0386	0.3282	0.2028
C−O	+0.11	0.0612	−0.0800	−0.0347	0.2985	0.1838
	+0.15	0.0630	−0.0774	−0.0571	0.2615	0.1270
	+0.30	0.1097	−0.1769	−0.1580	0.3820	0.0471
	+0.50	0.2541	−0.4897	−0.4707	0.3947	−0.5658
	+0.70	0.3101	−0.6577	−0.6200	0.8170	−0.4607
	CH_2(O)SH(2)	0.3122	−0.6649	−0.6269	0.8345	−0.4573

[a] *S*: reaction coordinate in unit of (amu)$^{1/2}$ bohr. [b] A minus sign denotes reverse direction of the reaction; a plus sign denotes forward direction of the reaction. [c] $\nabla^2\rho$: Laplacian of electron density.

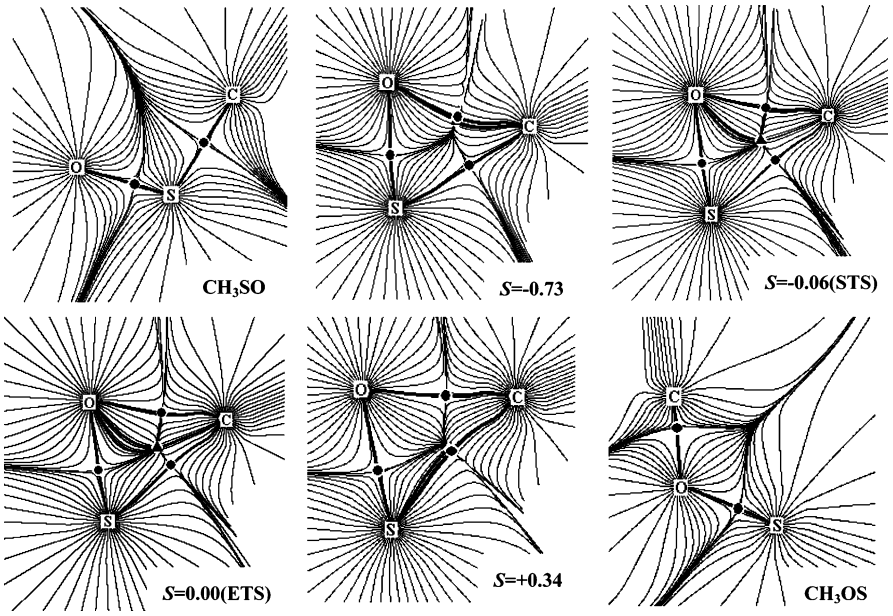

Figure 4. Contour maps of electronic density and gradient path of density surface of CH_3SO → CH_3OS reaction (▲ represents bond critical point, and ● represents ring critical point).

$CH_2OSH \xrightarrow{TS5} CH_2SOH$. The S atom is displaced from the C−H−O plane and the C atom is displaced from the H−O−S plane about 14.3 and 25.7 degrees, respectively. It is the first time we found out that the four atoms which formed the four-membered ring structures are not in the same plane. Our study results extended the concept of four-membered ring structures from one plane to a near-plane.

In the CH(OH)SH(1) $\xrightarrow{TS7}$ CH_2(O)SH(2) process, from CH(OH)SH(1) to $S_c = -0.12$, the S−O bond becomes more and more weak, the bond path becomes more and more bent, and the S−O bond path slides along the O−H bond. At the point $S_c = -0.11$, there is a bond path between sulfur atom and the BCP of the O−H bond. After that point, the S−H bond formed. Then, the O−H bond path begins to slide along the S−H bond,

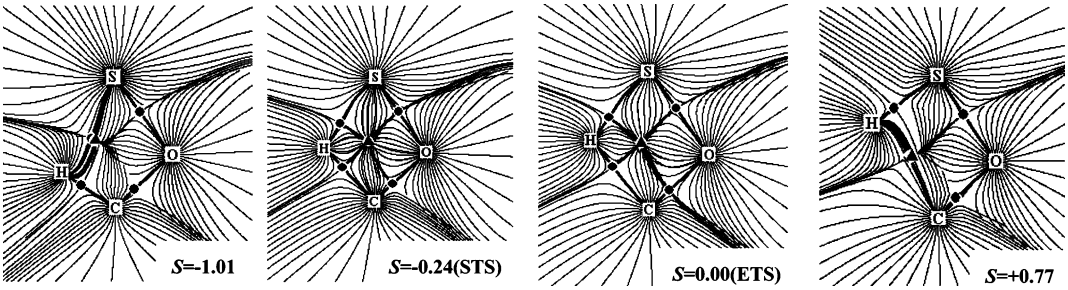

Figure 5. Contour maps of electronic density and gradient path of density surface of $CH_3OS \rightarrow CH_2OSH$ reaction (▲ represents bond critical point, and ● represents ring critical point).

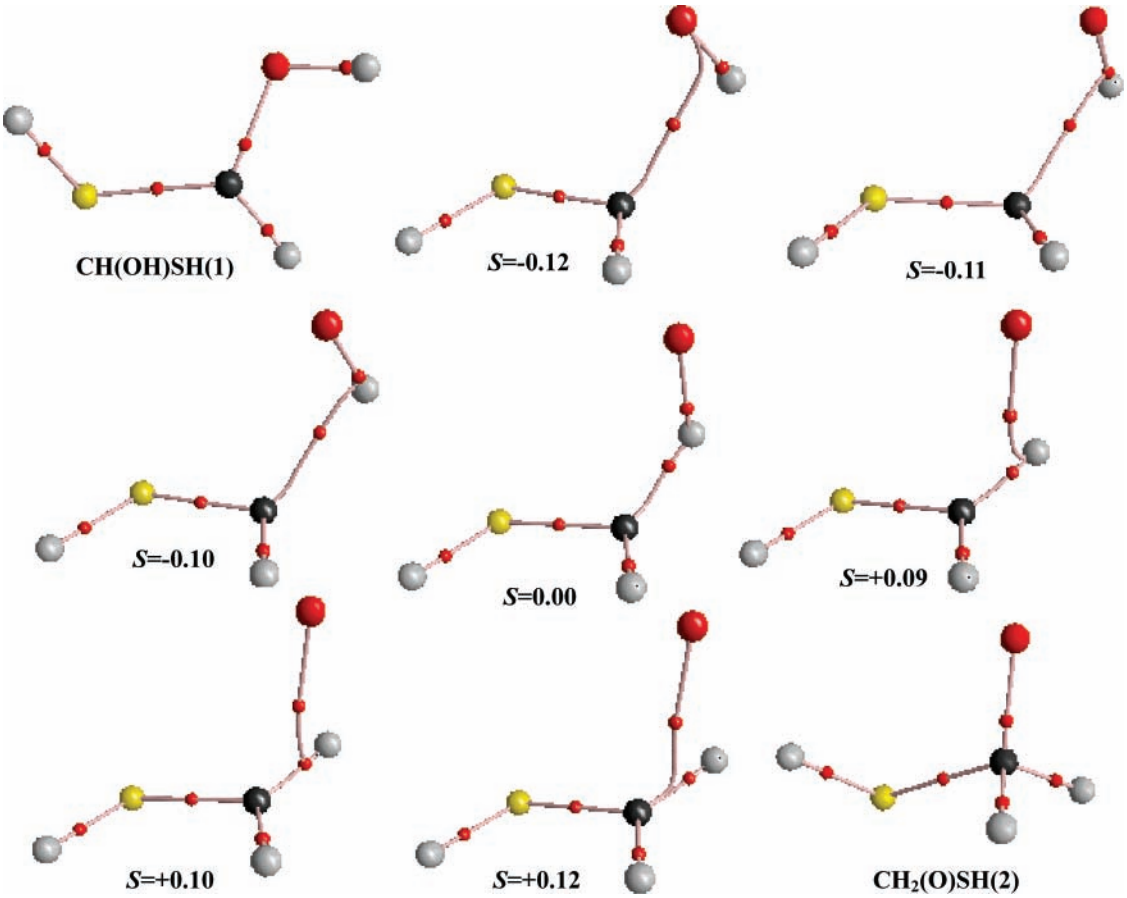

Figure 6. Molecular graph of $CH(OH)SH(1) \rightarrow CH_2(O)SH(2)$ reaction.

and at the point of $S_c = +0.10$, there is a bond path between the oxygen atom and the BCP of the S−H bond. After $S_c = +0.10$, an O atom links to a S atom and the S−O bond formed. Then the S−O bond becomes stronger and stronger and CH_2-(O)SH(2) formed.

3.2.2. Structure Transition State and Structure Transition Region. When an old bond is broken and a new bond is formed, the structure transition state (STS) and structure transition region (STR) will appear.[20,21] There are two kinds of STS. One is a kind of T-shaped conflict structure transition state that includes a bond path linking a nucleus and a bond critical point (BCP). We call it the first kind of structure transition state. The other is a kind of bifurcation-type ring structure transition enveloped by some bond paths and three or more nuclei. As the RCP just appears, the RCP is very close to the BCP of the newly formed bond. As the process proceeds, the RCP moves to the center of the ring. When the RCP goes to the BCP of another bond, this bond is broken and the ring disappears. From the ring's appearance to its disappearance, called the structure transition region, the λ_2 eigenvalue of the Hessian Matrix of the RCP (the positive curvature lying in the plane) has the trend of zero to maximum to zero. We refer to the maximum Hessian Matrix λ_2 of the RCP as STS and to the traditional transition state that is the maximum on the energy surface as the energy transition state (ETS).

Both kinds of structure transition states appear in the nine isomerization reaction. A three-membered ring structure appears in the five isomerization, a four-membered ring structure in the three isomerization, and the T-shaped STS exists in one isomerization. We observed that at $S_c = -0.11$ and $S_c = +0.10$ for $CH(OH)SH(1) \xrightarrow{TS7} CH_2(O)SH(2)$ are T-shaped conflict STSs. There is a bifurcation-type three-membered ring structure transition region for these processes: $S_a = -0.73$ to $S_a = +0.34$ for $CH_3SO \xrightarrow{TS1} CH_3OS$ process, $S = -0.54$ to $S = -0.20$ for $CH_2SOH \xrightarrow{TS4} CH_2S(O)H$ process, $S = +0.04$ to $S = +0.08$ for $CH(OH)SH(1) \xrightarrow{TS6} CH_2(O)SH(2)$ process, $S = +0.04$ to $S = +0.08$ for $CH(OH)SH(2) \xrightarrow{TS8} CH_2(O)SH(3)$ process, and $S = -0.41$ to $S = -0.19$ for $CH_3SO \xrightarrow{TS9} CH_2S(O)H$ process.

Four-membered ring structure transition region for these processes: $S_b = -1.01$ to $S_b = +0.77$ for $CH_3OS \xrightarrow{TS2} CH_2OSH$ process, $S = -1.08$ to $S = -0.48$ for $CH_3SO \xrightarrow{TS3} CH_2SOH$ process, and $S = -0.80$ to $S = +0.91$ for $CH_2OSH \xrightarrow{TS5} CH_2SOH$ process. In the eight transition structure region, $S_a = -0.06$, $S_b = -0.24$, $S3 = -0.70$, $S4 = -0.41$, $S5 = +0.12$, $S6 = +0.06$, $S8 = +0.06$, and $S9 = -0.31$ are the STS points of these processes.

Figure 3 also gives the position of the STS, ETS, and the transition-state region along the reaction pathways. The position of STS is not the position of ETS. In the $CH_3SO \xrightarrow{TS1} CH_3OS$, $CH(OH)SH(1) \xrightarrow{TS6} CH_2(O)SH(2)$, $CH(OH)SH(1) \xrightarrow{TS7} CH_2(O)SH(2)$, and $CH(OH)SH(2) \xrightarrow{TS8} CH_2(O)SH(3)$ process, the reaction energy is small, and the STS is near to the ETS. But in other reactions with apparent change between the products and the reactant, the STS is far from the ETS. That is, the lower the reaction energy is, the nearer the STS is to the ETS.

4. Conclusions

(1) For the CH_3SO system, 11 isomers are located. CH_3SO, $CH_2(S)OH$, CH(OH)SH(1), and CH(OH)SH(2) are stable in the 11 isomers, and the other 7 isomers are unstable; CH_2OSH and $CH_2S(O)H$ are the most unstable isomers.

(2) There are two kinds of STS in the isomerization reactions: the T-shaped conflict STS and the three- and four-membered ring STS.

(3) The near-plane four-member ring STS is found in our study. It is the first time we found that atoms which form the ring STS are not in the same plane. Our finding extended the concept of ring STS.

(4) The position of STS is not the position of ETS. The lower the reaction energy is, the nearer the STS is to the ETS.

Acknowledgment. This project was supported by the National Natural Science Foundation of China (Contract No: 20573032, 20503035), the Natural Science Foundation of Hebei Province (Contract No. B2006000137, B2006000131). X.L. thanks the Chinese Academy of Sciences for a scholarship for the period of this work.

References and Notes

(1) Barone, S. B.; Turnipseed, A. A.; Ravishankara, A. R. *Faraday Discuss.* 1995, *100*, 39.

(2) Turnipseed, A. A., Ravishankara, A. R. *Dimethylsulfide*: *Oceans, Atomphere and Climate*; Restelli, G., Angeletti, G., Eds.; Proceeding of the International Symposium held in Belgirate, Italy, 13-15 October 1992; Kluwer Academic: New York, 1992; p 185.

(3) Ravishankara, A. R.; Rudich, Y.; Talukdar, T.; Barone, S. B. *Philos. Trans. R. Soc. London, Ser. B* **1997**, *352*, 171.

(4) Li, X. Y.; Zeng, Y. L.; Meng, L. P.; Zheng, S. J. *Acta Chim. Sin. B* **2005**, *63*, 352.

(5) Kukui, A.; Bossoutrot, V.; Laverdet, G.; Bras, G. L. *J. Chem. Phys. A* **2000**, *104* (5), 935.

(6) Turecek, F.; Drinkwater, D. E.; Mclafferty, F. W. *J. Am. Chem. Soc.* **1989**, *111* (20), 7696.

(7) Dominé, F.; Ravishankara, A. R.; Howard, C. J. *J. Phys. Chem.* **1992**, *96*, 2171.

(8) Hung, W. C.; Shen, M. Y.; Lee, Y. P.; Wang, N. S.; Cheng, B. M. *J. Chem. Phys. B* **1996**, *105* (17), 7402.

(9) Dominé, F.; Murrells, T. P.; Howard, C. J. *J. Phys. Chem. B* **1990**, *94* (15), 5839.

(10) Borissenko, D.; Kukui, A.; Laverdel, G.; Bras, G. L. *J. Chem. Phys.* **2003**, *107* (8), 1155.

(11) Glukhovtsev, M. N.; Pross, A.; Mcgrath, M. P.; Radom, L. *J. Chem. Phys.* **1995**, *103*, 1878.

(12) Gonzalez, C.; Schlegel, H. B. *J. Chem. Phys.* **1989**, *90*, 2154.

(13) Gonzalez, C.; Schlegel, H. B. *J. Chem. Phys.* **1990**, *94*, 5523.

(14) Frisch, M. J.; Trucks, G. W.; Schlegel, H. B.; Scuseria, G. E.; Robb, M. A.; Cheeseman, J. R.; Zakrzewski, V. G.; Montgomery, J. A., Jr.; Stratmann, R. E.; Burant, J. C.; Dapprich, S.; Millam, J. M.; Daniels, A. D.; Kudin, K. N.; Strain, M. C.; Farkas, O.; Tomasi, J.; Barone, V.; Cossi, M.; Cammi, R.; Mennucci, B.; Pomelli, C.; Adamo, C.; Clifford, S.; Ochterski, J.; Petersson, G. A.; Ayala, P. Y.; Cui, Q.; Morokuma, K.; Malick, D. K.; Rabuck, A. D.; Raghavachari, K.; Foresman, J. B.; Cioslowski, J.; Ortiz, J. V.; Stefanov, B. B.; Liu, G.; Liashenko, A.; Piskorz, P.; Komaromi, I.; Gomperts, R.; Martin, R. L.; Fox, D. J.; Keith, T.; Al-Laham, M. A.; Peng, C. Y.; Nanayakkara, A.; Gonzalez, C.; Challacombe, M.; Gill, P. M. W.; Johnson, B.; Chen, W.; Wong, M. W.; Andres, J. L.; Gonzalez, C.; Head-Gordon, M.; Replogle, E. S.; Pople, J. A. *GAUSSIAN 98*; Gaussian Inc.: Pittsburgh, PA, 1998.

(15) Biegler-König, F. *AIM 2000*, Version 1.0; University of Applied Science: Bielefeld, Germany, 2000.

(16) Bader, R. F. W.; Tang, T.-H.; Tal, Y.; Biegler-König, F. W. *J. Am. Chem. Soc.* **1982**, *104*, 946.

(17) Alikhani, M. E. *Chem. Phys. Lett.* **1997**, *277*, 239.

(18) Bader, R. F. W. *Atoms in Molecules*—A Quantum Theory; Oxford University Press: Oxford, 1990.

(19) Bader, R. F. W. *Chem. Rev.* **1991**, *91*, 893.

(20) Zeng, Y. L.; Zheng, S. J.; Meng, L. P. *J. Phys. Chem. A* **2004**, *108*, 10527.

(21) Zeng, Y. L.; Zheng, S. J.; Meng,. L. P. *Inorg. Chem.* **2004**, *43*, 5311.